JOURNAL OF COMPUTATIONAL PHYSICS 76, 385–413 (1988)

Solution of the Diffusion Equation by Finite Elements in Lagrangian Hydrodynamic Codes

A. I. SHESTAKOV, J. A. HARTE, AND D. S. KERSHAW

Computational Physics Division, Lawrence Livermore National Laboratory, P.O Box 5508, Livermore, California 94550

Received January 15, 1987, revised July 14, 1987

The radiation diffusion equation is solved by the finite element method. The energy densities are point centered. These are integrated into a program architecture which requires zonally averaged quantities. Numerical results are presented which compare the scheme with existing finite difference techniques for zonal variables. Finite elements give better results for transport dominated problems on non-orthogonal meshes such as might be generated by Lagrangian hydrodynamic distortions

1. INTRODUCTION AND MOTIVATION

Kershaw [1] described finite difference schemes which use zonally averaged quantities. These schemes may cause anomalously large transport when used on sufficiently non-orthogonal grids. Such grids commonly appear in practice; they may also be generated from distortions due to Lagrangian hydrodynamics. The impetus for pursuing the present work is to devise a method which is more independent of mesh irregularities.

The finite element method (FE) has given accurate results over irregular domains. In this paper FE is applied to a parabolic equation on an irregular grid. Specifically, the radiation diffusion equation is solved on a moving Lagrangian mesh. If the radiation field is nearly isotropic, an integration over the angle of propagation reduces the equation for the photon energy density to parabolic form. In our application the relevant equations are

$$\frac{du_\nu}{dt} = \nabla \cdot (D_\nu \nabla u_\nu) + \gamma_\nu (B_\nu(T_e) - u_\nu) + P \tag{1}$$

$$c_v \frac{dT_e}{dt} = -\alpha \int d\nu\, \gamma_\nu (B_\nu(T_e) - u_\nu) + Q, \tag{2}$$

where u_ν, the radiation energy density per frequency group, and T_e, the electron temperature, are the dependent variables. The cylindrical variables (R, Z) and the photon frequency, ν, are the independent variables. Inclusion of the Fokker–Planck

0021-9991/88 $3.00

approximation for scattering [2] introduces a second-order operator in frequency space in Eq. (1) that is applied to u_ν. Since the operator depends on T_e, self-consistency requires that the energy changes in the radiation field due to scattering be reflected in the electrons. This adds a corresponding term to Eq. (2). In this paper we ignore scattering effects and simply define the diffusion coefficient, D_ν, and the coupling coefficient γ_ν in terms of the photon absorption mean free path, l_ν:

$$D_\nu = cl_\nu/3 \qquad \text{and} \qquad \gamma_\nu = c/l_\nu, \tag{3}$$

where c is the speed of light. Assuming local thermodynamic equilibrium, $\gamma_\nu = c\rho\kappa_\nu$ where ρ is the mass density and κ_ν is the absorption opacity. The photon total mean free path is the inverse of the sum of $\rho\kappa_\nu$ and the scattering coefficient σ_s [2]. In the following, we set $\sigma_s = 0$ and use the definitions in Eqs. (3). Time is normalized to $\tau = 10^{-8}$ s, all distances are in *centimeters*; hence $c = 300$. The mean free path l_ν and the specific heat c_ν are given by an equation of state; $B_\nu(T_e)$ is the Planck function. Both ν and T_e are in keV; u_ν has units of keV^3 per cm^3 while $\alpha = 0.00211$ is a normalizing constant in units of energy per keV^4. Energy is measured in units of 10^{16} ergs. The Lagrangian time derivative on the lhs of Eqs. (1) and (2) is approximated by time-differencing the variables on a mesh that moves with the fluid.

The terms P and Q denote other physical processes such as electron–ion coupling, radiation PdV work, and scattering which are solved by operator splitting. Their solution is not discussed here, but the effects are incorporated into the scheme as external sources.

Except for the linearization of B given below, fully implicit time differencing is used in order to ensure numerical stability and to avoid the oscillations that can occur for short wavelength modes [1]. In most applications, u_ν quickly equilibrates with the matter ($\gamma_\nu \gg 1$). Fully implicit time differencing is able to obtain what is effectively a succession of steady states of u_ν, states that vary with changes in the boundary conditions. In particular, in the limit of infinite time steps, the scheme computes the steady state answer in one time step. Schemes such as Crank–Nicholson require several time iterations to reach the desired state.

In the following, the subscript "e" for the electron temperature is dropped. Let T^n and u^n respectively denote the numerical value of the temperature and the radiation energy at the end of the nth time level; neglect the operator P. Given T^{n-1}, operator splitting for Q generates an intermediate temperature $T'^{,n-1}$; the latter is advanced to T^n by coupling to the radiation field. The frequency spectrum is discretized into N_ν groups. Let u_{ν_i} denote the average energy in the ith group; the energies are coupled by the temperature equation. The "partial temperature scheme," which we now describe, reduces Eqs. (1) and (2) to N_ν systems of two scalar equations. Assume that each u_{ν_i} contributes separately to the temperature change, $T^n - T'^{,n-1}$:

$$T^n - T'^{,n-1} = T_{N_\nu} - T_{N_\nu - 1} + T_{N_\nu - 1} - \cdots + T_1 - T_0, \tag{4}$$

where $T_{N_v} = \bar{T}^n$, $T_0 = T'^{,n-1}$, and T_i is the intermediate temperature due to the coupled advancement to u_{v_i}. This results in the N_v equations:

$$\frac{u^n - u^{n-1}}{\Delta t} = \nabla \cdot (D \nabla u^n) + \gamma (B(T_i) - u^n) \tag{5}$$

$$c_v \frac{T_i - T_{i-1}}{\Delta t} = -\alpha \Delta v \gamma (B(T_i) - u^n), \tag{6}$$

where the subscripts v_i are dropped. Equations (5) and (6) are solved N_v times per time step, once for each group energy, u_{v_i}. Each solution computes a new "partial T_i."

The contribution to the integral in Eq. (2) has been approximated by a midpoint rule in Eq. (6). The Planck function is proportional to $v^3(\exp(v/T_e) - 1)^{-1}$; its integral to T^4,

$$\int_{v_{i-1}}^{v_i} B_v(T)\, dv = T^4 \int_{v_{i-1}/T}^{v_i/T} x^3\, dx/(e^x - 1).$$

The group energies are advanced in random order in order to minimize biasing the solution. For example, consider the extreme case in which energy is copiously added to only one group u_{v_k}. If the energies were advanced in a monotonic order, e.g., increasing v_i, all groups for which $v_i < v_k$ would be unaffected by the energy deposition until the subsequent time step. The calculation may develop significant errors if (as is commonly the case) these "lower" groups are tightly coupled to the matter due to their short mean free path.

In the partial temperatue scheme, the Planck function is linearized about the latest temperature,

$$B(T_i) = B(T_{i-1}) + \frac{dB(T_{i-1})}{dT}(T_i - T_{i-1}) \tag{7}$$

and this is substituted into Eqs. (5) and (6). The linearization renders Eq. (6) linear in $T_i - T_{i-1}$. One solves for this temperature change and substitutes the result into Eq. (5). The result is a scalar equation involving u^n and known quantities of the form,

$$\Delta t^{-1}(u^n - u^{n-1}) = \nabla \cdot (D \nabla u^n) - \beta u^n + s \tag{8}$$

with $\beta \geqslant 0$.

Although the scheme is stable, Δt is governed by accuracy considerations. Controls are provided which decrease Δt if either $(T^n - T^{n-1})/T^{n-1}$ or $(T_i - T^{n-1})/T^{n-1}$ exceed specified tolerances. Indeed, such restrictions are required to render Eq. (7) a good approximation.

In our program, the mesh coordinates are labeled by logical K, L variables:

$Z(K, L)$, $R(K, L)$, with $1 \leqslant K \leqslant KMAX$ and $1 \leqslant L \leqslant LMAX$. In (K, L) space the grid is rectangular; in (R, Z) space, the mesh consists of quadrilaterals. Azimuthal symmetry is assumed. The program environment external to the processes described here require, and possibly update, zonally averaged values; c_v and l are constant in a quadrilateral. For example, P and Q use zonal quantities. In contrast, the FE computes nodal values for u and T. An important part of this paper is to integrate these nodal calculations into other zonal physics.

The following section describes how the finite element method is applied to the solution of Eqs. (5) and (6). Sections 2.1 and 2.2 discuss the solution of Eq. (8). The necessity of coupling the nodal representation of u to a similar representation for T_e is proved in Section 2.3. Section 2.4 presents the numerical analog of physical terms such as the energy exchanged with the matter. Section 3 describes several procedures required to couple the radiation diffusion package to other zone centered physics equations; the section is only tangentionally linked with the principal subject of this paper. Nevertheless, it contains numerical results which are important in order to successfully integrate the scheme into a larger Lagrangian environment. Four test problems are presented in Section 4. The FE results are compared with analytic solutions or with the finite difference scheme [1]. Section 5 is a conclusion.

2. Implementation of the Finite Element Method

2.1. *Discretization of Equation*

Each quadrilateral zone is bisected into triangles. Triangulation strategies are discussed below. Since coefficients such as l and c_t are piecewise constant on zones, hence piecewise constant on triangles, only linear finite elements are used. Since distinct quadrilaterals may define different materials, with correspondingly extreme changes in l_v, it would be incorrect to impose smoothness of derivatives of the trial functions [3].

Specifically, if $KL = KMAX * LMAX$ denotes the total number of mesh points, consider the function space

$$F = \{\phi_j(R, Z)\}_{j=1}^{KL}.$$

Each element of F is of the form $\phi_j = a_j + Rb_j + Zc_j$. The coefficients are chosen so that ϕ_j equals unity at the jth grid point and vanishes at all other grid points. By construction, ϕ_j is identically zero on triangles which do not have the jth grid point as a vertex. The unknown functions are given in terms of the basis functions $\phi_j(\mathbf{x})$,

$$u^n = \sum_{j=1}^{KL} u_j^n \phi_j \qquad \text{and} \qquad T^n = \sum_{j=1}^{KL} T_j^n \phi_j. \tag{9}$$

As previously mentioned, the program requires zonally averaged quantities which are supplied using

$$\langle u^n \rangle_i = \int_{q_i} u^n R\, dR\, dZ \Big/ \int_{q_i} R\, dR\, dZ, \tag{10}$$

where q_i denotes the ith quadrilateral. Note the extra R factor in the metric. The physical processes P of Eq. (1) such as Compton scattering and $P\,dV$ work do not involve any spatial derivatives. The same operator splitting methods which were applied to $\langle u^n \rangle_i$ are now applied to u_j^n. On the other hand, process Q of Eq. (2) introduces coupling to the ion temperature, a zonal quantity. We show below that if T is left as a zonal variable, and coupled to a nodal u in the obvious way, that physically relevant choices for l_v lead to anomalously large transport due to numerical diffusion. Consequently, T must also have a point-centered representation.

Equations (5) and (6) hold in some domain Ω with boundary $\partial\Omega$. The FE is implemented using the "weak" form of the pde, that is, each of the equations is multiplied by ϕ_k for $k = 1, ..., N$ and integrated over the domain, where N ($\leqslant KL$) is the number of unknown grid values. Equation (6) is discretized analogously. "Lumping" [3], which is described below, allows us to solve for the unknown temperature change as in the previous discussion. This is substituted into the weak form of Eq. (5) and eliminates the unknown T^n. This gives the weak form of Eq. (8),

$$2\pi \int_\Omega \phi_k [\Delta t^{-1}(u^n - u^{n-1}) - \nabla \cdot (D \nabla u^n) + \beta u^n - s]\, R\, dR\, dZ = 0, \tag{11}$$

where u^n is defined in Eq. (9) and $k = 1, ..., N$. Any sources or sinks of radiation of the form $\sigma_1 - \sigma_2 u$ added to the rhs of Eq. (5) are easily assimilated into Eq. (11). The transport term is integrated by parts,

$$-\int_\Omega \phi_k \nabla \cdot (D \nabla u^n)\, R\, dR\, dZ = -\int_{\partial\Omega} \phi_k\, D\, \hat{\mathbf{n}} \cdot \nabla u^n\, R dl + \int_\Omega D\, \nabla \phi_k \cdot \nabla u^n\, R\, dR\, dZ, \tag{12}$$

where $\hat{\mathbf{n}}$ is the unit outward normal, and dl is the incremental arc length.

Since u^n is given by Eq. (9), Eq. (11) leads to a linear system

$$\mathbf{A}\mathbf{x} = \mathbf{b} \tag{13}$$

for the unknowns $\{u_j^n\}$. Part of $\mathbf{A}$ consists of the stress matrix, $\mathbf{S}$, whose elements are

$$S_{kj} = \int_\Omega D\, \nabla \phi_k \cdot \nabla \phi_j\, R\, dR\, dZ.$$

This matrix is symmetric and non-negative definite. It can be shown that if all triangles have interior angles $\leqslant \pi/2$, that the diagonal elements S_{kk} are positive and off-diagonal elements are non-positive. In this case, **S** is an M-matrix and monotone [4]; i.e., $\mathbf{S}^{-1}$ has all positive elements. A triangulation strategy which minimizes the occurrence of obtuse angles enhances positivity of $\mathbf{S}^{-1}$.

Positivity is desirable from a physical standpoint. In Eq. (13), **x** denotes the vector of unknown energy densities u_j^n which are meaningful only if positive. The rhs depends on u_j^{n-1}. The matrix **A** is a sum of $\Delta t\mathbf{S}$ and a multiple of the mass matrix, i.e., the matrix resulting from discretizing the term $\int \phi_k u^n$. In contrast to finite difference schemes, strict adherence to the u^n representation of Eq. (9) gives a nondiagonal mass matrix since

$$\int_\Omega \phi_k\, u^n\, R\, dR\, dZ = \sum_j \left(\int_\Omega \phi_k\, \phi_j\, R\, dR\, dZ \right) u_j^n.$$

Trial functions, ϕ_j, whose support intersects the support of ϕ_k yield positive off-diagonal mass matrix elements. By "lumping" one approximates

$$\int_\Omega \phi_k\, u^n\, R\, dR\, dZ \to u_k^n \int_\Omega \phi_k\, R\, dR\, dZ.$$

The resulting matrix is diagonal with positive diagonal elements. The signs of all the terms multiplying the mass matrix, Δt^{-1} and β, add to the diagonal dominance of **S**, **A** is positive definite for any triangulation and an M-matrix if no triangle has an interior angle larger than $\pi/2$.

2.2. *Boundary Conditions*

On $\partial\Omega$ three possible conditions arise;

(a) Dirichlet condition, $u = u_b$ along $\partial\Omega_1$,

(b) Neumann condition, $-D\partial u/\partial n = u_f$ along $\partial\Omega_2$ or

(c) mixed or "Milne" condition, $u + (2l/3)\,\partial u/\partial n = u_m$ along $\partial\Omega_3$,

where $\partial\Omega_i$ is a subset of $\partial\Omega$. Physically, either the radiation energy, the flux, or a Milne condition is being specified. If $u_m = 0$, then (c) states that the outgoing flux equals c times one-half the energy at the boundary. The latter is the correct physical condition to impose at a vacuum interface.

The implementation of these conditions is straightforward. If (a) is given and $\mathbf{x}_{j1}$ is a grid point on $\partial\Omega_1$, then $k \neq j1$ in Eq. (11). If N_1 such grid points lie on $\partial\Omega_1$, then $N = KL - N_1$ is the number of unknowns. In this case, $u(\mathbf{x}_{j1})$ is a given boundary condition. However, u and T are each still given by KL grid values, Eq. (9). The new temperature values T^n need to be computed on $\partial\Omega_1$.

If condition (b) or (c) is given, then $D\partial u/\partial n$, is given in terms of u_f or u_m. The value is substituted into the line integral of Eq. (12). Lumping is used if a Milne condition is specified. Condition (b) or (c) is assumed to be piecewise constant on

the line segments between grid points lying on $\partial\Omega_2$ or $\partial\Omega_3$, whereas Dirichlet conditions hold on points.

In all cases, the integration is performed only over Ω, the domain of interest. There are N unknowns to compute for u_j^n; order $(\mathbf{A}) = N$.

2.3. *Necessity of Nodal Description of T*

In this section, we demonstrate the importance of defining both u and T as nodal functions. This necessity is proved analytically and verified computationally in a model problem. The result is not needed for the subsequent sections.

In our application, zonal quantities need to be supplied to other processes at the end of the time step. Since the only spatial derivatives in Eqs. (5) and (6) appear in the $\nabla\cdot(D\nabla u)$ term, one might reason that only a nodal representation of u is sufficient and that T may retain its zonal description.

Consider the following model problem. In the limit of small l, the transport term is insignificant. Set $D=0$ in Eq. (5) and assume a linear Planck function,

$$B(T) = B_0 + B_0'(T - T_0),$$

where T_0, B_0, and B_0' are constants. After changing variables, in the limit of small Δt, Eqs. (5) and (6) become

$$\partial_t r = \gamma(B_1 e - r) + c_0 \tag{14a}$$

$$\partial_t e = -\gamma(B_1 e - r) - c_0, \tag{14b}$$

where r and e respectively denote the radiation and electron energies ($r = \alpha\Delta v u$, $e = c_v T$) and B_1 is the ratio of specific heats ($B_1 = \alpha\Delta v B_0'/c_v$). Note that the hydrodynamic effects are also neglected.

Assume that Eqs. (14) hold for $0 \leqslant x \leqslant X_{\max}$, and $t > 0$, with given initial conditions and set $c_0 = 0$. In the context that e is a zonal variable and r is known on points, the FE may be applied as follows. Given a discretization $\{x_j\}$, consider the "tent" functions $\{\phi_j(x)\}$, where $\phi_j(x)$ is linear in x and $\phi_j(x_i) = \delta_{ij}$. Furthermore, define $\phi^{\pm}(x)$, where ϕ_j^- and ϕ_j^+ are respectively the left and right halves of ϕ_j; i.e., $\phi_j^-(x) = 0$ if x does not belong to $(x_{j-1}, x_j]$, and $\phi_j^+(x) = 0$ if x does not belong to $[x_j, x_{j+1})$. Since r is given on points, $r = \{r_j\}$ while $e = \{e_{j+1/2}\}$ where

$$e_{j+1/2}(x_{j+1} - x_j) = \int_{x_j}^{x_{j+1}} e.$$

Use implicit time differencing in Eqs. (14) and form three equations for $\int \phi_j r$, $\int \phi_j^+ e$, and $\int \phi_{j+1}^- e$. Using lumped mass matrices for r, $\int \phi_j r(x) = r_j \int \phi_j$. The implicit equations for r_j^{n+1} and $e_{j+1/2}^{n+1}$ can be inverted to give the linear system,

$$r_j^{n+1} = a_j e_{j-1/2}^n + b_j r_j^n + c_j e_{j+1/2}^n \tag{15a}$$

$$e_{j+1/2}^{n+1} = d_j e_{j-1/2}^n + f_j r_j^n + g_j e_{j+1/2}^n + h_j r_{j+1}^n + i_j e_{j+3/2}^n \tag{15b}$$

where the coefficients a, b, ..., depend on Δx, Δt, etc. These equations are equivalent to solving the following system with an explicit difference scheme

$$\partial_t r = \beta(B_1 e - r)$$
$$\partial_t e = -\beta(B_1 e - r) + \Delta t \Delta x^2 \beta\gamma B_1 \partial_{xx} e/4d,$$

where $\beta = \gamma(1 + \gamma\Delta t(1 + B_1))^{-1}$ and $d = 1 + \gamma\Delta t\, B_1$. The scheme has a numerical diffusion coefficient which may also be expressed as

$$D_n = \Delta t\, \Delta x^2 \gamma^2\, B_1/4p(\gamma\Delta t),$$

where $p(z)$ is quadratic in z, $p(0) = 1$, $\lim_{z\to\infty} p(z) = +\infty$. The numerical diffusion is innocuous; if it is dominated by the physical diffusion coefficient D as defined in Eq. (3),

$$\frac{D_n}{D} = \frac{3}{4}\left(\frac{\Delta x}{l}\right)^2 \frac{\gamma\Delta t B_1}{p(\gamma\Delta t)}.$$

Note that $D_n/D \ll 1$ if $\Delta t \ll 1$, $\Delta t \gg 1$, or $\Delta x \ll l$. The last inequality usually is not satisfied since the diffusion limit of the radiation transport equation is derived assuming a short mean free path. If $l \ll \Delta x$, the above analysis signals that D_n may dominate for some cases if Δt is chosen appropriately. The cases arise, if the ratio of specific heats, $B_1 \gg (\Delta x/l)^2 \gg 1$.

This analysis is verified computationally. Restore the transport term in Eq. (14a) and consider the system

$$\partial_t r = \partial_x(D\partial_x r) + \gamma(Be - r) + b \tag{16a}$$
$$\partial_t e = -\gamma(Be - r) - b, \tag{16b}$$

where b, B, and l are constant; l is used to define D and γ as in Eq. (3). The boundary conditions model symmetry at the left and a vacuum on the right:

$$\partial_x r = 0 \quad \text{at} \quad x = 0 \qquad \text{and} \qquad r + \frac{2l}{3}\partial_x r = 0 \quad \text{at} \quad x = 1.$$

The exact solution is

$$r_e = \sum r_i(t) \cos k_i x$$

$$e_e = -(b/\gamma B) + \sum e_i(t) \cos k_i x,$$

where k_i, $i = 1, 2, \ldots$, solve

$$\cot k = 2lk/3.$$

The Fourier coefficients solve the system

$$\frac{d}{dt}\begin{bmatrix} r_l \\ e_l \end{bmatrix} = \gamma \begin{bmatrix} -B & 1 \\ B & -1-k_l^2 D/\gamma \end{bmatrix} \begin{bmatrix} r_l \\ e_l \end{bmatrix}.$$

Thus, $r_l, e_l \sim e^{\lambda t}$ where

$$\lambda_{\pm} = (2B)^{-1}[-1-B-k_l^2 D/\gamma \pm (4B + (B-1-k_l^2 D/\gamma)^2)^{1/2}].$$

Define the total energy and energy change,

$$E(t) = \int_0^1 (r(x,t) + e(x,t))\, dx = -(b/\gamma B) + (2l/3) \sum (r_l(t) + e_l(t)) \cos k_l.$$

The energy change is obtained by adding Eqs. (16) and integrating

$$\Delta E = E(t) - E(0) = -(c/2) \sum \cos k_l \int_0^t r_l(s)\, ds.$$

Since energy leaves the problem only at $x = 1$, a numerically computed ΔE consists of both the physical transport losses and anomalous numerical diffusion. As l decreases, the transport term in Eq. (16a) becomes less significant and the energy lost at $x = 1$ is correspondingly smaller. A method with a large numerical diffusion coefficient will let energy escape at a faster rate. The above analysis predicts that a nodal u coupled to a zonal T will be inaccurate if $\Delta x \gg l$.

Two 1D test programs were written to solve Eqs. (16). The first, ZT, uses zone centered temperatures, the second, PT, defines e (equivalently T) on points. The radiation energy r is always defined on points. The programs were initialized using only one eigenfunction, $\cos k_1 x$. The following parameters were used: $B_1 = 2$, $l = 3 \times 10^{-4}$; hence $D = 3 \times 10^{-2}$ and $\gamma = 10^6$.

The initial energy $E(0) = 4.45512$. Both programs used $\Delta x = 10^{-2}$, thus $(\Delta x/l)^2 \approx 10^3$. Three successively increasing values of $\gamma \Delta t$ are used; these choices assume that the second one falls in the range where the analysis predicts $D_n \gg D$.

TABLE I

Comparison of Energy Diffusion between Zonal (ZT) and Nodal (PT) Schemes

Run	Prog.	$\gamma \Delta t$	N_t	ΔE_e	ΔE	D_n/D
1	PT	10^{-3}	10^4	-4.711×10^{-9}	-4.854×10^{-9}	
1	ZT	10^{-3}	10^4	-4.711×10^{-9}	-1.045×10^{-8}	1.6×10^{-2}
2	PT	8.33×10^{-2}	10^3	-3.926×10^{-6}	-3.926×10^{-6}	
2	ZT	8.33×10^{-2}	10^3	-3.926×10^{-6}	-4.384×10^{-4}	95.33
3	PT	10^4	10^2	-4.597×10^{-2}	-4.596×10^{-2}	
3	ZT	10^4	10^2	-4.597×10^{-2}	-4.782×10^{-2}	2.7×10^{-2}

The programs are run N_t cycles, the numerical energy change, ΔE, is computed and compared with the exact value, ΔE_e. Results are given in Table I. Note that for the second run, $D_n/D \approx 100$ which is approximately the amount of extra energy that exited the problem in the time allowed. We conclude that T must be a nodal variable as in Eq. (9).

2.4. *Energy Conservation, Edit Quantities*

The FE scheme conserves the same quantities as the differential equations. In this section, we derive precise analogs for the change in radiation energy, for the energy transported, for the energy coupled, etc. First consider global quantities. At each point where u is to be computed, Eq. (5) becomes

$$\int_\Omega (\phi_k(u-u^0-\gamma\Delta t(B-u)) + \Delta t\, D\,\nabla\phi_k\cdot\nabla u)\, R\, dR\, dZ = \Delta t \int_{\partial\Omega} \phi_k D\nabla u\cdot\hat{\mathbf{n}}\, R\, dl, \quad (17)$$

where $k = 1, ..., N$ and N is the total number of unknown grid values u_k. The old grid function is marked with a superscript. Define

$$\Phi = \sum_{k=1}^{N} \phi_k(R, Z).$$

If there is no Dirichlet data, $\Phi = 1$ throughout Ω, otherwise, $\Psi = 1 - \Phi$ defines a piecewise linear function which equals 1 at the Dirichlet grid points and vanishes at the others. Sum Eq. (17) for $k = 1, ..., N$, then

$$\int \Phi(u-u^0) = \Delta t\left[\int (\Phi\gamma(B-u) - D\,\nabla\Phi\cdot\nabla u)\, R\, dR\, dZ + \int \Phi D\nabla u\cdot\hat{\mathbf{n}}\, R\, dl\right]. \quad (18)$$

Add $\int \Psi(u-u^0)$ to both sides (note $1 = \Phi + \Psi$), then

$$\int (u-u^0) = \Delta t \int \gamma(B-u) + \int [\Psi(u-u^0-\gamma\Delta t(B-u)) + \Delta t\, D\,\nabla\Psi\cdot\nabla u] + \Delta t \int \Phi D\nabla u\cdot\hat{\mathbf{n}}\, R\, dl. \quad (19)$$

Multiplication by $\alpha\, \Delta v$ converts the units into energy. The lhs is the global energy change during the time step. The rhs respectively consists of the total energy exchange with the matter, the energy necessary to maintain u at its prescribed value (the Dirichlet data), and the energy escaped through the walls. The sign of the energy escaped depends on the Neumann or mixed boundary condition. Since the FE equations are also applied to Eq. (6) at every grid point, these can also be summed for all $\phi_k(\mathbf{x})$, $k = 1, ..., KL$,

$$\int c_v(T-T^0) = -\alpha\Delta v\, \Delta t \int \gamma(B-u). \quad (20)$$

Thus, the first integral on the rhs of Eq. (19) is more conveniently computed from the change in electron energy, i.e., the lhs of Eq. (20). This is modified if T is given a prescribed value.

One likewise has pointwise energy conservation. Consider Eq. (17), where $\mathbf{x}_k$ is an interior grid point. On the lhs, the first term is the energy change; the second or analogously $\int \phi_k c_v(T-T^0)$, is the energy exchanged, and $\int \Delta t\, D\nabla\phi_k \cdot \nabla u$ is the energy transported. The rhs of Eq. (17) vanishes when $\mathbf{x}_k$ does not fall on $\partial\Omega$. Each of the above terms must be computed as they were discretized. For example, for lumped mass matrices,

$$\int \phi_k(u-u^0) = (u_k - u_k^0)\int \phi_k .$$

One may also derive conservation relations for subregions contained in Ω. Assume for simplicity that Ω' is a closed subregion whose boundary does not intersect $\partial\Omega$. Let

$$\Theta = \sum_k \phi_k,$$

where the sum is taken only over the functions ϕ_k corresponding to grid points $\mathbf{x}_k$ lying in Ω' or its boundary. Hence, $\Theta = 1$ throughout Ω' and drops sharply to zero in one "mesh width" surrounding Ω'. Substituting Θ for Φ in Eq. (18) gives

$$\int_{\Gamma+\Omega'} \Theta(u-u^0) = \Delta t \int_{\Gamma+\Omega'} \Theta\gamma(B-u) - \Delta t \int_{\Gamma} D\nabla\Theta\cdot\nabla u. \tag{21}$$

where Γ is a narrow strip surrounding Ω'. The boundary term of Eq. (18) vanishes since $\Theta = 0$ on $\partial\Omega$. Equation (21) states that the energy change equals that exchanged with the electrons plus the flux transported through the "surface" of the volume, Γ. Consider two quadrilaterals, q_i, with vertices $A, \ldots, F$, Fig. 1. Assume $\Theta = 1$ at points C, D and vanishes at the other vertices. Then,

$$F_1 \equiv \Delta t \int_{q_1} D\nabla\Theta\cdot\nabla u$$

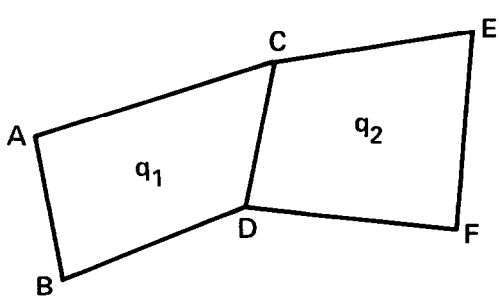

FIG. 1. Two adjoining quadrilaterals.

is the energy flux entering q_1 from q_2. It need not equal

$$F_2 \equiv \Delta t \int_{q_2} D \nabla \Theta \cdot \nabla u,$$

the flux entering q_2 from q_1. Since the flux across the line CD is required, we average, $F = (F_1 + F_2)/2$, to define the flux between the two zones. These flux edits are computed from the stress matrix elements, S_{kj} a posteriori.

3. Coupling of FE to Other Physics

This section describes procedures required to conform with a Lagrangian environment in which the variables have zonal definitions.

3.1. *Retriangulation*

In the FE formulation, each quadrilateral is bisected into triangles. Initially, the possibly nonorthogonal quadrilaterals are bisected by a strategy which strives to guarantee a stable and accurate difference approximation (see below). However, Lagrangian hydrodynamics distorts the mesh. Some quadrilaterals may become so distorted as to cause the integration routines to compute negative areas for the triangles. The mesh is monitored, and retriangulated if necessary. Retriangulation must be accompanied by redefining the nodal variables, u_j and T_j, in order to conserve energy.

Consider retriangulating one quadrilateral, Fig. 2. Let $u = \sum_{j=1}^{4} u_j \phi_j(\mathbf{x})$ and $u' = \sum_{j=1}^{4} u'_j \psi_j(\mathbf{x})$ respectively denote the representation before and after retriangulating. We seek the values u'_j that minimize $E = \int (u - u')^2 \, d\mathbf{x}$, with the constraint that energy be conserved, i.e., $\int u \, d\mathbf{x} = \int u' \, d\mathbf{x}$. The integrals are done over the quadrilateral. If λ is a Lagrange multiplier; minimize $E + 2\lambda \int (u - u')$ with respect to $u' = (u'_l)_{l=1}^{4}$ for some value λ. The minimization gives the system

$$\mathbf{M}\mathbf{u}' - \mathbf{N}\mathbf{u} - \lambda \boldsymbol{\omega}' = 0, \tag{22}$$

where $M_{k,l} = (\int \psi_k \psi_l)$, $N_{k,l} = (\int \psi_k \phi_l)$, and $\omega'_j = \int \psi_j$. Equation (22) is solved for $\mathbf{u}'$ and dotted with $\boldsymbol{\omega}'$. If $\omega_l = \int \phi_j$, the constraint implies $\boldsymbol{\omega}' \cdot \mathbf{u}' = \boldsymbol{\omega} \cdot \mathbf{u}$. This

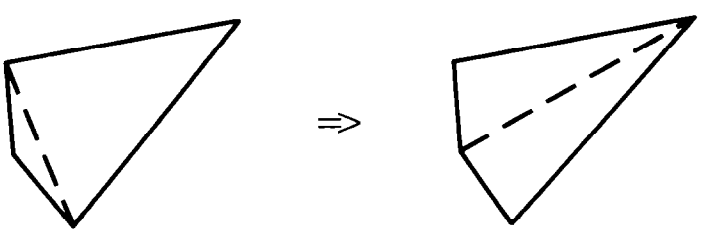

FIG. 2. Retriangulation of quadrilateral.

substitution gives an equation for λ; the result can be expressed as a linear system for the new point values,

$$\mathbf{M}\mathbf{u}' = \mathbf{N}\mathbf{u} + (\boldsymbol{\omega}' \cdot \mathbf{M}^{-1}\boldsymbol{\omega}')^{-1}(\boldsymbol{\omega} \cdot \mathbf{u} - \boldsymbol{\omega}' \cdot \mathbf{M}^{-1}\mathbf{N}\mathbf{u})\,\boldsymbol{\omega}'.$$

The procedure can be modified if instead of the L^2 norm, one minimizes the H^1 norm.

If several quadrilaterals need to be retriangulated, the algorithm is extended. In general, each grid point, $\mathbf{x}_j$, is a vertex of four quadrilaterals q_i, $i = 1, ..., 4$. Four copies of u_j, $(u_{ji})_{i=1}^4$, of each grid value are made. The above algorithm generates new grid values u'_{ji} on quadrilaterals requiring retriangulation. The new grid values are recombined by averaging,

$$u'_j \int \psi_j = \sum_{i=1}^{4} u'_{ji} \int \psi_{ji}, \tag{23}$$

where support $(\psi_{ji}) = i$th quadrilateral. Equation (23) is appropriately modified for the old nodal temperature since $c_v T$ is the quantity to be conserved.

The following criterion is used to determine if a zone warrants retriangulating. Each quadrilateral is first bisected according to its existing prescription, then bisected according to the opposite one. For each case the radius of the smaller inscribed circle is computed. The two radii are then compared. Let $r_{\min,1}$ and $r_{\min,2}$ respectively denote the minimum radii for the existing and opposite triangulation and let s_w be a constant. If $r_{\min,1} < s_w r_{\min,2}$ a zone is tagged for retriangulation. The switch factor, s_w, is an input quantity. Clearly, $0 < s_w \leqslant 1$. Values of $s_w \approx 1$ may cause an undesirable number of retriangulations and lead to numerical diffusion. Typically, $s_w = 0.8$. Experience has shown that if s_w is too small (≈ 0.5), the triangles may get significantly distorted before they are retriangulated. These distortions cause large obtuse angles destroying the M–matrix property of the diffusion matrix, $\mathbf{S}$; see Section 2.1.

3.2. *Zonal–Nodal Temperature Mapping*

At the end of the time step, the nodal values u_j^n and T_j^n are stored. The required zonal quantities are obtained from Eq. (10). A number of processes may alter the zonal temperature before the start of the next radiation cycle. For example, Q in Eq. (2) may consist of sources of energy to the electrons. Other changes to T may be due to PdV work on the electrons by the hydrodynamics. Another example is subtler. The program strives to conserve energy. Electron energies, zonal quantities, are stored. These change as the calculation proceeds, e.g., the radiation field exchanges energy with the electrons. Although a problem may consist of several materials, each with its own equation of state, EOS, zones demarcate them. Thus, one node may be at the boundary of disparate materials. If left unchecked, the zonal temperature may stray from the value necessary to give an EOS value, $E(T, \rho)$ that agrees with the stored zonal energy. Consequently, at the start of each

cycle, one Newton iteration of the following equation is made to "redefine" the zonal temperature

$$E - E_{\text{EOS}} = \frac{dE}{dT}(T'_z - T_z). \tag{24}$$

In Eq. (24), the lhs is the difference between the zonal electron energy and its EOS value; energy exchanged with the radiation is a constituent of E. The rhs of Eq. (24) multiplies the zonal heat capacity by the necessary temperature difference; T'_z is the new zonal temperature.

At the start of the radiation transport these changes need to be reflected in the nodal values, i.e., a mapping from the zones to the points. Such a mapping is extraneous to the main theme of this paper, and the subject did not arise in any of our idealized test problems. However, the mapping is a crucial part of any "real" physics calculation. Experience has shown how seemingly reasonable choices lead to disaster. The difficulty may be appreciated by a 1D example.

Assume an infinite domain discretized by a constant mesh width $\Delta x = 1$. Let $T'_{j+1/2}$ denote the result of Eq. (24); it represents the zonal temperature for $j \leqslant x \leqslant j+1$. Assume $T'_{j+1/2}$ is zero everywhere except $T'_{1/2} = 1$, and that $dE/dT = 1$ everywhere. Ideally, one desires a nodal temperature T'_j $(= T(x_j)$, where $x_j = j)$ which is generated by $T'_{j+1/2}$ and returns this value after the point to zone mapping Eq. (10). For the $T'_{j+1/2}$ described above, the result is unacceptable and obviously non-physical since $T'_0 = 1$, $T'_j = 1$ if $j = 2k-1$, and $T'_j = -1$ if $j = 2k$, where $j = 1, 2, 3, \ldots$. A similar sawtooth behavior is found for negative indices. A better choice would be $T'_j = \frac{1}{2}$ if $j = 0, 1$ and zero for all other values. Yet, this diffuses the temperature difference in one zone to three. Subsequently, iterations of Eq. (24) in later cycles try to realign the zonal temperature and introduce other sawtooth profiles. The difficulty lies in attempting to express a discontinuous (zonal) function, T'_z, by a continuous (nodal) one, T'_j.

The scheme presented below has allowed us to obtain useful results on "real" problems, yet it does share some of the undesirable sawtooth behavior described above. Work on improvements is continuing.

The radiation cycle occurs after the Lagrangian displacement of the mesh. New basis functions are computed using the old triangulation prescription. The convection of radiation is accomplished by dividing the old radiation energy at a point, $u_j \int \phi_j^0$, by the newly computed basis function, $\int \phi_j$. Retriangulation and subsequent redefinition of the nodal values is then done to obtain a better discretization of the domain. Let u_j^n, T_j^n denote these nodal values, and let T_z^n denote the zonal average of T_j^n per Eq. (10). In general, T_z^n does not equal T'_z, the result of Eq. (24). The zonal temperature difference $\Delta T = T'_z - T_z^n$ must be broadcast to the points.

The mapping maps the zonal energy change, $(dE/dT)_z \Delta T$, to the points. Sawtooth behavior is minimized by passing the result through a filter which does not allow the creation of local extrema unless they are present in T_j^n or T'_z. In 1D

let $T^n_{J+1/2}$ and $T'_{J+1/2}$ represent the zonal temperatures. Define the zonal specific heat, $c_{v,J+1/2}$,

$$(x_{J+1} - x_J)\, c_{v,J+1/2} = (dE/dT)_{J+1/2}$$

and the point heat capacity,

$$a_J = \int \phi_J c_v.$$

An intermediate nodal temperature, T'_J, is computed using

$$a_J(T'_J - T^n_J) = c_{v,J-1/2}(T'_{J-1/2} - T^n_{J-1/2}) \int_{x_{J-1}}^{x_J} \phi_J + c_{v,J+1/2}(T'_{J+1/2} - T^n_{J+1/2}) \int_{x_J}^{x_{J+1}} \phi_J. \tag{25}$$

This equation may generate unphysical extrema. Physical extremal values are determined from the old and new zonal temperatures,

$$T_{J,x} \equiv \max(T^n_J,\ T'_{J\pm 1/2}) \qquad \text{and} \qquad T_{J,n} \equiv \min(T^n_J,\ T'_{J\pm 1/2}). \tag{26}$$

These are used to filter the results of Eq. (25):

$$T^{n'}_J = \begin{cases} T_{J,x}, & \text{if} \quad T'_J > T_{J,x} \\ T_{J,n}, & \text{if} \quad T'_J < T_{J,n} \\ T'_J, & \text{otherwise.} \end{cases} \tag{27}$$

The filter violates energy conservation. However, the single iteration of Eq. (24) for T'_z does not generate an energy conserving temperature either. Thus, we rely on subsequent time steps to converge to the correct T. In a rapidly changing problem, the temperature will be out of alignment with the energy. Boundary conditions modify the extremal filters used in Eq. (27).

The mapping concludes by computing a temperature change per group,

$$\Delta T^n_J = (T^{n'}_J - T^n_J)/N_\nu,$$

where N_ν is the number of frequency groups. The partial temperature scheme, which cycles through the groups, advances $T^n_J + \Delta T^n_J$ to obtain the temperature at the end of the cycle. In this manner, large temperature changes are distributed continuously to the groups. That is, if the ith group is being computed then $T^n_J + \Delta T^n_J$ is used to obtain the intermediate temperature T_i—see discussion following Eq. (4).

3.3. *Flux Limiter and Positivity Controls*

In this section, we describe several features of the diffusion package required to obtain physically acceptable results. The radiation diffusion equations are derived

in the limit of near isotropy. Thus, the radiation mean free path, l_ν, should be considerably shorter than the characteristic length scale of the problem. Nevertheless, these equations can give meaningful results in other regimes. Consequently, the equations are modified in order that they not violate physical expectations. The radiation flux, $D\nabla u$, must be bounded by the limit imposed if all the energy were to flow in one direction, e.g., cu. However, if l_ν is longer than the characteristic gradient length of u ($\nabla u \approx u/d$), anomalously large flux results and $D\nabla u/cu \gg 1$. The diffusion coefficient is modified as

$$D = \begin{cases} c/(3/l + \max(0, |\nabla u|/u)) & \text{or} \\ c/\max(3/l, |\nabla u|/u), \end{cases} \tag{28}$$

where l and u depend on ν. The coefficient D is constant on each triangle; u in Eqs. (28) is the average value on the triangle (equal to one-third the sum of its nodal values). The coefficient is explicit, i.e., at the nth time level, u^{n-1} is used to evaluate D. The term, $\max(0, |\nabla u|/u)$ in Eq. (28) maintains D positive; it turns off the flux limiter whenever u is negative. The second alternative of Eq. (28) generates more flux. It compares better to some 1D transport calculations for optically thin problems ($l_\nu \gg \Delta x$).

Flux limiters are only tangentionally involved with our presentation yet they are principal subjects of entire other papers. The reader interested in this subject is directed to the works of Levermore and Pomraning [5] and Levermore [6] and to the references cited therein. Flux limiters, such as those suggested by Levermore, will be incorporated in the FE program.

Negative energies often arise at the foot of steep fronts whenever the mesh is badly skewed, since the resulting matrix may no longer be monotone. Two choices allow the user to control the calculation. One scans the energies after they have been computed and zeroes those values which are negative. The other examines the energies before they are advanced and zeroes the coupling coefficient, γ_ν, wherever the old energy densities are negative. The effect of the first removes the unphysical values from the problem. It gives good results on some problems. However, it violates energy conservation as the negative values are the algebraically correct solutions to the discretized operator. Excessive usage may generate "reasonable" solutions yet the energy check may show errors of order 1. The second choice has the heuristic appeal that the unphysical negative energies are not allowed to drag down T_e. Hopefully, the positive energies that constitute the thermal front will diffuse and raise the negative values above zero. However, for thermal wave problems similar to those described in the next section, we instead observe that the spurious negative values propagate out ahead of the wave effectively lowering the radiation temperature, T_r in the material; T_r then is out of equilibrium with T_e and, as discussed above, the zeroed coupling coefficient prevents equilibration. We prefer the first choice, but monitor the energy check.

The problem of minimizing the occurrence of negative energies is considered by Pert [7] who scans the diffusion matrix and modifies elements that may give

unphysical extrema. We instead strive to generate monotone matrices. Lumped mass matrices and a triangulation strategy that minimizes the occurrence of obtuse angles inhibits the generation of negative values. However, if some arise, the choices cited above are provided.

4. Numerical Results

Here we present and compare FE with FD, the zonal finite difference scheme described in Ref. [1]. In the first subsection, three problems with known analytic solutions are computed. In the second, a multigroup calculation is presented. The units used are those described in Section 1 ($c = 300$).

4.1. *Idealized Test Problems*

Three test problems are presented in order of increasing complexity. For these cases, the mesh is fixed but "random." It is depicted in Fig. 3 where $0 \leqslant R, Z \leqslant 1$; Z is the abscissa and R is the ordinate. A total of 33×33 grid points are initialized. The initial and boundary conditions are those of a 1D problem. The purpose is to determine what effect the distorted mesh has on the solution. Only one frequency group is considered; operators P and Q in Eqs. (1) and (2) are neglected.

In the first two examples, $\gamma = 0$ and $l = 0.055$; i.e., only linear radiation diffusion is modeled. The grid is defined by a logical rectangle of (K, L) lines.

For the first problem, we compute the steady state solution which is linear in Z. In this case, FE computes the exact solution regardless of mesh distortion. We use $KMAX = LMAX = 33$, the lines $K = 1$ and $KMAX$ respectively define $R = 1$ and 0

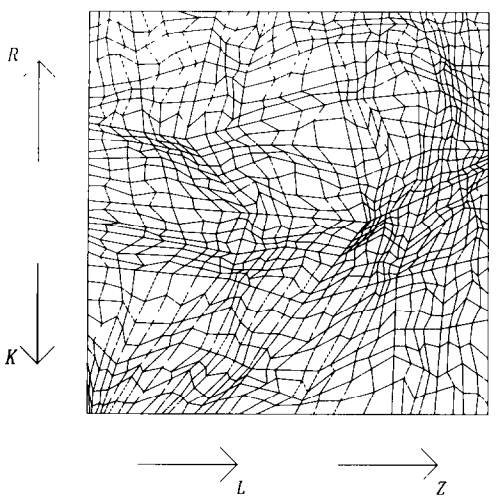

FIG. 3. Random grid on unit square in (R, Z) space; Z is the abscissa, R is the ordinate.

while the lines $L=1$ and $LMAX$ define $Z=0$ and 1. The initial condition is $u \approx 0$. Boundary conditions are $\partial u/\partial n = 0$ at $R=0$ and $K=1$, and $u=1$ at $Z=1$. A Milne condition, $u+(2l/3)\ \partial u/\partial n = 0$, holds at $Z=0$. In Fig. 4, the steady state flux, $D\partial u/\partial n$, is plotted vs. K along $Z=0$. Note the variation of the FD solution. FE is a dramatic improvement; however, this is not a fair comparison due to the linearity of the steady state solution which FE is guaranteed to compute.

In the second problem, neither method is exact. We compute diffusion in spherical symmetry,

$$\partial_t u = (1/r^2)\ \partial_r((cl/3)\ r^2\ \partial_r u),$$

where r is the spherical radius. The computational domain is $0 \leqslant r \leqslant 1$ and $\pi/4 \leqslant \theta \leqslant \pi/2$, where θ is the polar angle. Symmetry conditions hold at $\theta = \pi/4$, $\pi/2$ and a Milne condition is imposed along $r=1$; at $r=0$, $\partial_r u = 0$. The problem is initialized with the analytic eigenfunction which is determined using separation of variables. Let

$$u = V(r)\ W(t); \tag{29}$$

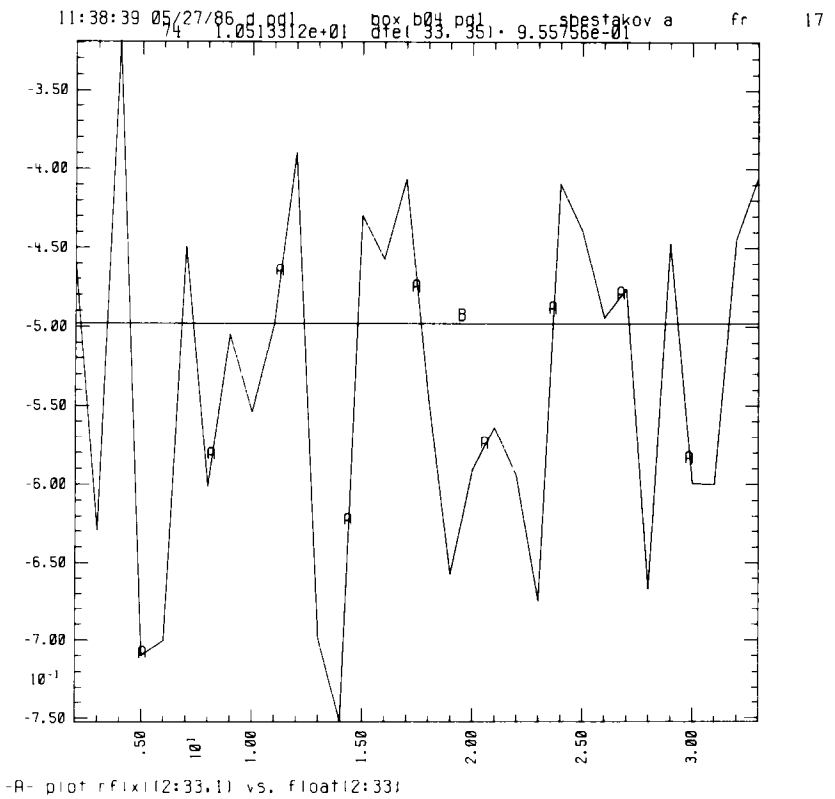

FIG. 4. Problem 1. Steady state flux vs index K along $Z=0$; A – FD solution, B – FE solution.

V solves a second-order ode and

$$W = W_0 e^{-clt d^{2.3}}. \tag{30}$$

Changing variables, $x = dr$, $y = r^{1/2}V$, gives Bessel's equation,

$$x^2 y'' + xy' + (x^2 - (\tfrac{1}{2})^2)\, y = 0.$$

The solution $J_{1/2} \sim x^{-1/2} \sin x$ satisfies the boundary condition at $r = 0$. The Milne condition, $V + (2l/3)\, V' = 0$ gives the equation for d,

$$\tan d = -2ld/3. \tag{31}$$

We choose the first positive root; using $l = 0.005$, $d = 3.1311558464015$. In terms of r,

$$V(r) = r^{-1/2}\, y(x) = d^{-1/2}\, r^{-1} \sin dr. \tag{32}$$

The solution is given by Eqs. (29), (30), and (32). The total energy is

$$E(t) = 2\pi \int_0^1 r^2\, u(r, t)\, dr \int_{\pi/4}^{\pi/2} \sin\theta\, d\theta = (-\sqrt{2}\pi(1 + 2l/3)\, d^{-3/2} \cos d)\, W(t),$$

after invoking Eq. (31). If $W_0 = 1$,

$$E(0) \equiv E_0 \equiv 0.8045062671.$$

The calculation is run until $t_1 = 0.20113777 \approx$ one e-folding time. The remaining energy is

$$E(t_1) \equiv E_1 = 0.3730693\, E_0 = 0.3001366.$$

The flux along $r = 1$ is

$$S_1(t) = -\frac{cl}{3}\, \partial_r u|_{r=1} = \left(-\frac{cl}{3}\, d^{1/2}(1 + 2l/3) \cos d\right) W(t)$$

in units of energy per square centimeters per time. At $t = t_1$,

$$S_1(t_1) = 0.8876544479\ W(t_1) = 0.3311567. \tag{33}$$

The above analytic solution is compared with computer runs which are obtained on a "random" mesh. The initial time step is $\Delta t_0 = 10^{-3}$, but the program increases the time step by 10% if the temperatures do not vary much. The runs conclude after 32 cycles, when Δt has grown to 0.0191943. Although some discrepancies between the numerical and analytic results may be due to the implicit temporal differencing, variations from spherical symmetry are due to the distorted mesh. The

improvement in FE over FD is demonstrated by comparing the final fluxes along $r = 1$ on the random meshes.

The grid is generated by a mapping

$$R_1 = R_0/\sqrt{1+Z_0^2}, \qquad Z_1 = Z_0 R_0/\sqrt{1+Z_0^2}, \tag{34}$$

where $0 \leqslant R_0, Z_0 \leqslant 1$. The random grid of Fig. 3 generates another in the region: $0 \leqslant \sqrt{R_1^2+Z_1^2} \leqslant 1$ and $\pi/4 \leqslant \tan^{-1}(R_1/Z_1) \leqslant \pi/2$. Figure 5 displays the new grid. The mapping concentrates more points near the $\theta = \pi/4$ boundary.

This example demonstrates the versatility of the FE subroutine. Since nodal values are computed, some modification of the matrix is required at the "center

of the energy density are computed. The modification ensures that all copies are equal. The fully implicit discretization of $u_t = \nabla \cdot (D\nabla u)$ generates a linear system, Eq. (13). The system is normalized by computing $a_s = \max_i(A_{ii})$, where A_{ii} are the diagonal elements. The system is then multiplied by a_s^{-1} ensuring that some

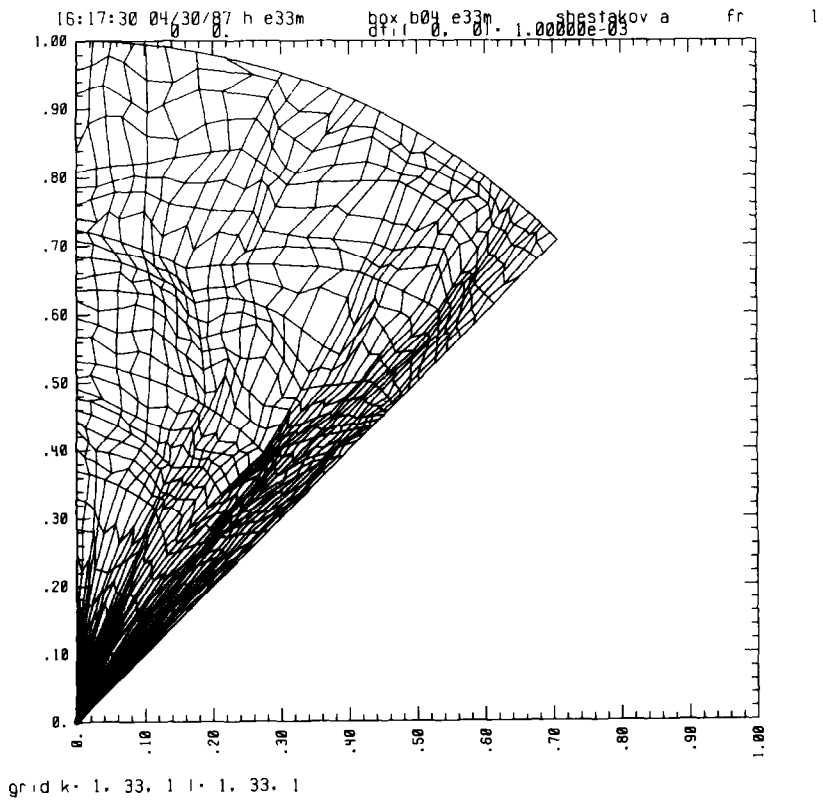

FIG. 5. Problems 2 and 3. Random computational grid; Z is the abscissa, R is the ordinate.

diagonal element equals one. To modify the matrix, assume the unknowns $\{u_i\}_{i=j}^{j+k}$ represent the k copies. Consider the ith equation,

$$\cdots b_{i-1}u_{i-1} + a_i u_i + b_i u_{i+1} + \cdots = s_i,$$

where $j+1 < i < j+k-1$. Since u_{i-1} should equal u_i, $10^6 a_{i-1}(u_{i-1} - u_i) = 0$ is added to the $i-1$th equation. This relationship and $10^6 a_i(u_i - u_{i+1}) = 0$ is also added to the ith; the modified ith equation is

$$\cdots (b_{i-1} - 10^6 a_{i-1})\, u_{i-1} + (a_i + 10^6 a_{i-1} + 10^6 a_i)\, u_i + (b_i - 10^6 a_i)\, u_{i+1} + \cdots = s_i.$$

Similar modifications are made to the remaining $k-j-1$ rows. Note that the matrix remains symmetric.

The fluxes along $r = 1$ are plotted in Fig. 6 for both FE and FD methods. Results were obtained on the 33×33 grid of Fig. 5. The FE energies are initialized with the analytic solution, Eq. (29), evaluated at the grid points. The initial FD energies are obtained by first computing the quadrilateral center as described by Kershaw [1, p. 377]. The analytic solution is then evaluated at those centers. Note the greater variation of FD in Fig. 6. Indeed, if F_x, F_n are respectively the maximum and minimum numerical values for the flux along $r = 1$, then the relative differences,

$$r_f = 2(F_x - F_n)/(F_x + F_n), \tag{35}$$

are respectively $r_{f,D} = 1.165$ and $r_{f,E} = 0.022$ for FD and FE. For comparison purposes, FD results on a 33×33 grid with constant Δr and $\Delta\theta$ give a flux of

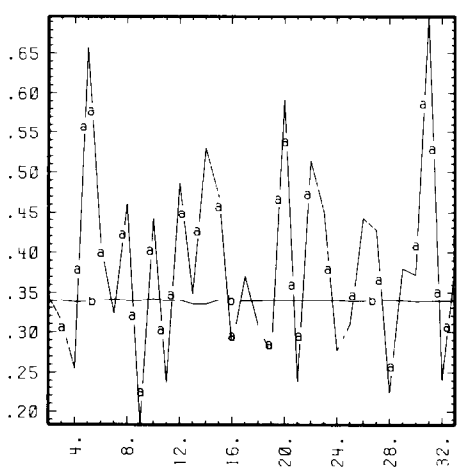

FIG. 6. Problem 2. Flux vs index L along $r = 1$; a – FD solution, b – FE solution.

$S_1 = 0.33943$. Differences between this and Eq. (33) are attributed to errors in Δt and to a lesser extent, mesh size.

The third test problem is a one-dimensional thermal wave. In Eqs. (1) and (2) neglect P and Q. Assume J is the basic unit of energy and α is in units of $J\,keV^{-4}$. Let $B_\nu(T) = \nu^3/(e^{\nu/T} - 1)$, in units of keV^3. Choose a sufficiently large ν_x to encompass the spectrum. Integrate Eq. (1) from 0 to ν_x, multiply by α and express

$$w \equiv \alpha \int_0^{\nu_x} u_\nu \, d\nu, \qquad \text{units}(w) = J.$$

Define a frequency averaged coupling coefficient,

$$\alpha \int d\nu \, \gamma_\nu (B_\nu(T) - u_\nu) = \gamma \left(\alpha T^4 \int_0^{\nu_x/T} \frac{x^3 \, dx}{e^x - 1} - w \right).$$

For large ν_x, and $T \leqslant 1$, $\int_0^{\nu_x/T} \approx \int_0^\infty = \pi^4/15$. These definitions reduce Eqs. (1) and (2) to a set of frequency averaged equations,

$$\partial_t w = \partial_z (D \partial_z w) + \gamma(\alpha_x T^4 - w) \tag{36}$$

$$c_v \, \partial_t T = -\gamma(\alpha_x T^4 - w), \tag{37}$$

where $\alpha_x = \alpha\pi^4/15 = 0.0137\, J\, keV^{-4}$; $D = cl/3$ and $\gamma = c/l$ are defined in terms of a frequency averaged mean free path, l.

Solve Eq. (37) for w, substitute the result into Eq. (36), and derive a single equation for T,

$$\partial_t \left(\frac{c_v}{\gamma} \partial_t T + \alpha_x T^4 + c_v T \right) = \partial_z \left[D \, \partial_z \left(\frac{c_v}{\gamma} \partial_t T + \alpha_x T^4 \right) \right]. \tag{38}$$

In the strong coupling limit,

$$\partial_t T \ll \gamma T, \tag{39}$$

the first term of Eq. (38) is dominated by the third; the case of small l. If the radiation energy is negligible when compared to the matter energy,

$$4\alpha_x T^3 \ll c_v, \tag{40}$$

the second term of Eq. (38) is dominated by the third. If the coupling time multiplied by the change of the matter energy with respect to time is dominated by the radiation energy,

$$\frac{c_v}{\gamma} \partial_t T \ll \alpha_x T^4, \tag{41}$$

the fourth term of Eq. (38) is dropped in favor of the fifth. Equations (39)–(41) reduce Eq. (38) to the thermal wave equation considered in Ref. [8],

$$\partial_t T = a\partial_z(T^3\partial_z T), \qquad a = 4\alpha_r cl/3c_v. \tag{42}$$

For the numerical test, Eqs. (5) and (6) are solved on the domain: $1 \leqslant R \leqslant 2$, $0 = Z_0 \leqslant Z \leqslant Z_2 = 2.09375$. Along $Z = Z_0$ and Z_2, $L = 1$ and $LMAX$; along $R = 1$ and 2, $K = KMAX$ and 1, respectively. In this problem $KMAX = 33$ and $LMAX = 68$. The grid is assembled from two 33×33 random meshes shown in Fig. 3: one for $0.00625 \leqslant Z \leqslant Z_1 = 1.0625$ and another for $1.09375 \leqslant Z \leqslant Z_2$. Elucidation for choosing such a domain follows. Only one frequency group is used, $\Delta v = v_x = 20$. The numerical flux is computed along the straight grid line $Z = Z_1$.

The solution for a plane source, $T(t=0) = Q\delta(z)$ is self-similar, and is given analytically [8]. It is characterized by a front position $z_f(t) \sim t^{1/5}$ and the value at the symmetry plane, $T_c \sim z_f^{-1}$. We choose $l = 0.001$ and $c_v = 50$; hence, $D = 0.1$, $\gamma = 3 \times 10^5$ and $a = 1.096 \times 10^{-4}$. Symmetry conditions ($\partial u/\partial n = 0$) are imposed along $R = 1$ and 2 and along Z_0. A Milne condition holds along $Z = Z_2$. The numerical solution loses physical significance when the front arrives at $Z = Z_2$. At $t = 0$, T and u are nonzero only along $Z = Z_0$. Initially, the functions are in equilibrium, $w = \alpha_r T^4$, and are independent of R. The thermal wave solution is completely determined once the total heat Q,

$$Q \equiv \int dz \left(T + \frac{w}{c_v} \right),$$

is specified, for this quantity is conserved by Eqs. (36) and (37). For the numerical domain, $Z = 0$ and $Z = \Delta Z = \frac{1}{32}$ are straight grid lines. In the range $0 \leqslant Z \leqslant \Delta Z$, ΔR ($= \frac{1}{32}$) is held constant. The random grid begins at $Z = 2\Delta Z$. This ensures that the total heat per point is independent of R at the initial time. Omitting this, i.e., starting the random grid at $Z = 0$ creates a thermal wave propagation velocity that is not independent of R for early times. Setting $T = T_c(t=0) = 1$ and zero everywhere else gives $Q = 0.031258562$. Since T only decays, the choice for c_v assures that Eq. (40) is always satisfied. Using the dimensional argument, $T \sim T_c \sim z_f^{-1} \sim t^{-1/5}$, we derive analogs of Eq. (39),

$$1 \ll 5\gamma t \tag{39a}$$

and of Eq. (41),

$$\frac{c_v}{\alpha_r} \ll 5\gamma t^{2/5}. \tag{41a}$$

The choice for c_v implies that Eq. (39a) holds whenever Eq. (41a) does. The latter implies

$$2.9 \times 10^{-7} \ll t.$$

That is, the solution of Eqs. (36) and (37) or equivalently Eqs. (5) and (6) will only fail to equal the solution of Eq. (38) at very early times. The numerical problem, however, may be considered to start not at $t=0$, but at that time for which $z_f=\frac{1}{32}$ which is considerably longer than the numerical value in the last equation.

A comparison of FE with the analytic solution is given in Figs. 7 and 8. Figure 7 plots the temperature vs. Z along $R=1$ at $t\approx 6.995\times 10^8$. The profile agrees with the analytic function. Figure 8 plots the time history of the flux across $Z=Z_1$. The numerical results of Fig. 8 display the radiation flux, f, vs. time, where

$$f=-2\pi\alpha\int_1^2 R\,dR\int_0^{v_1} D\nabla u\,dv.$$

The stong coupling assumption, Eq. (39a), implies $u\approx B(T)$. This gives an expression for f in terms of T,

$$f=-4\pi\alpha_v c l T^3\,\partial_z T.$$

The flux corresponding to Eq. (39) is $S=-aT^3\,\partial_z T$. Thus, $f=3\pi c_v S$. Along $Z=Z_1$, the analytic flux peaks at $t=7.522\times 10^8$ and $S_{\max}=2.1751\times 10^{-12}$ which translates to $f_{\max}=3\pi c_t\ S_{\max}=1.02499\times 10^{-9}$. At $t=7.5948\times 10^8$, FE computes a numerical flux of $f_{\max,\,\text{numer}}=9.969\times 10^{-10}$ or 2.7% less.

Running the FD scheme on this problem gave answers that also compared very well with the analytic function. The FD flux across $Z=Z_1$ peaks at $t\approx 7.9\times 10^8$ giving $f_{\text{numer}}\approx 1.02\times 10^{-9}$, very nearly the analytic maximum. However, a time history of the FD flux has an incorrect "double peaked" probile, the earlier peak occurring at $t\approx 6.7\times 10^8$ for which $f\approx 1.00\times 10^{-9}$. Computing the relative differences of the fluxes, Eq. (35), along $Z=Z_1$, FD gives $r_{f,D}=1.05$ at $t=6.89\times 10^8$ while FE gives $r_{f,E}=0.76$ at $t=6.99\times 10^8$. The improvement in symmetry by the FE scheme is noticeable but not as dramatic. We hypothesize that the strong coupling in this problem, $\gamma\gg D$, reduces the importance of accurately computing the transport term.

4.2. *Radiative Cooling of a Sphere of Hot Air*

In this section the FE and FD schemes are compared on a multigroup problem. We model the sudden cooling of a hot sphere of air by radiative transport [9]. The problem is simplified in order to underscore the differences in the performances of the two methods.

The domain consists of a similar spherical section as for the second problem except $0\leqslant r\leqslant 10$ cm, where r is the spherical radius. Boundary conditions are as before; symmetry holds along $\theta=\pi/4$ and $\pi/2$ and a Milne condition is imposed along the outer edge of the sphere. All physical processes except those described in Eqs. (1) and (2) are neglected. Runs are made on both an orthogonal mesh (constant Δr and $\Delta\theta$) and the random one described above. The flux limiter is shut off.

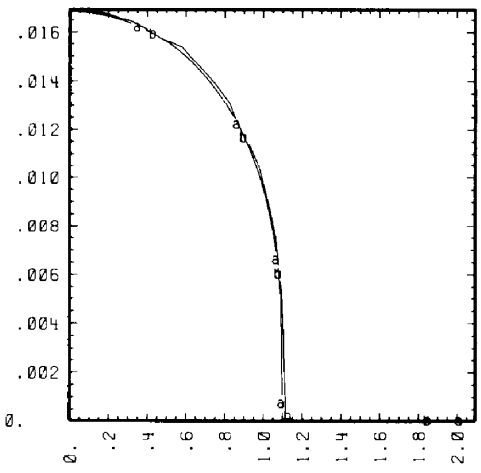

FIG 7 Problem 3. Temperature vs Z at $t = 6\,995 \times 10^8$; a – analytic solution, b – FE solution.

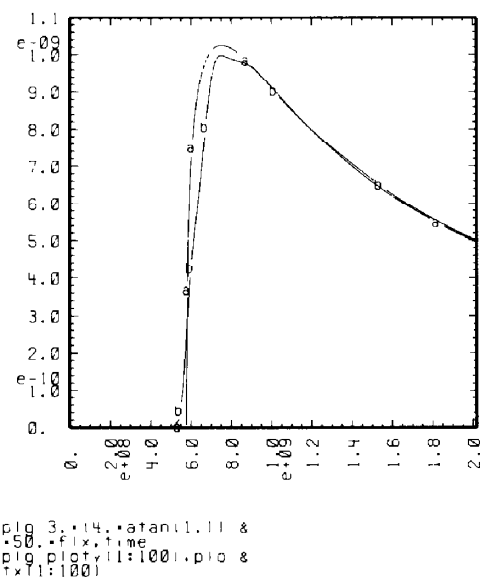

At $t = 0$, the radiation field is in equilibrium with the matter, $T_r = T_e = 0.9$ eV. At this temperature the matter is transparent to the bulk of the radiation. The opacities are those given Johnston and Stevenson [10]. Figure 9 displays κ_ν vs photon energy (i.e., frequency). The radiation field has the Planck distribution depicted in Fig. 10. The density is $\rho = 0.001293$ gm/cm^3. The Rosseland averaged mean free path is $l_R = 10.031$ cm. The problem is obviously dominated by transport. The initial energy in the radiation field is 1.331×10^5 ergs. The runs begin with $\Delta t = 10^{-6}$ and the time step is allowed to increase by 33% each cycle. The calculations are halted after 31 cycles at $t \approx 0.020933$. The photon energy spectrum is divided into 30 logarithmically spaced groups with $\nu_{MAX} = 0.2$ keV and $\nu_1 = 10^{-5}$ keV. Figure 9 shows that the opacities are not experimentally tabulated below $\nu = 10^{-4}$. Hence, we could run with a significantly higher value for ν_1. This has no effect on the comparisons; at the lower frequencies, the opacities are effectively independent of the frequency.

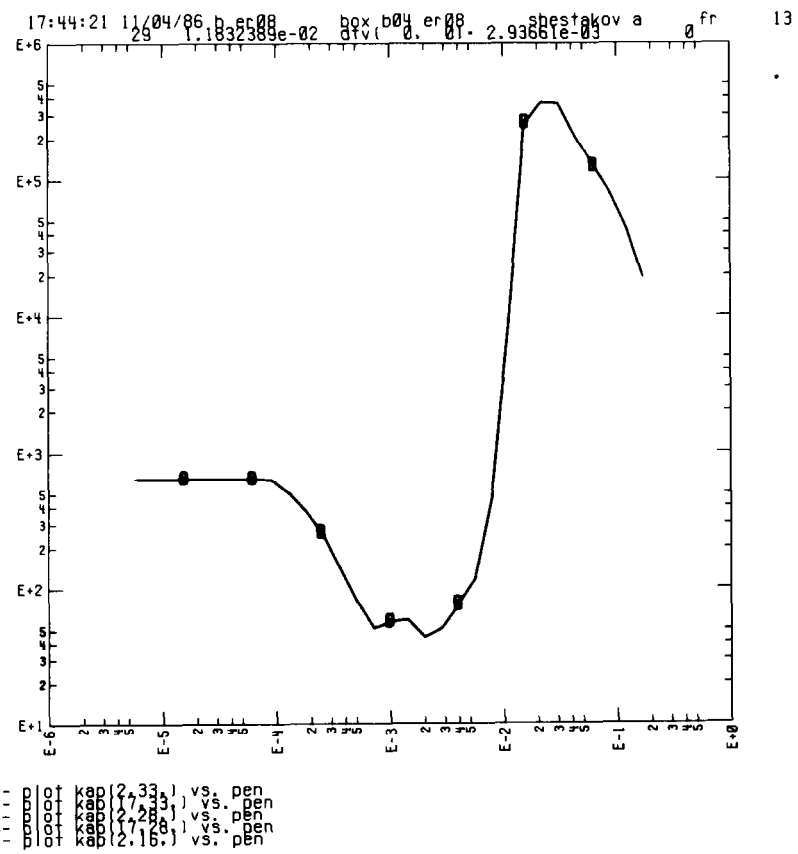

FIG. 9. Problem 4. Opacity (cm^2/g) is the abscissa, photon energy (keV) is the ordinate.

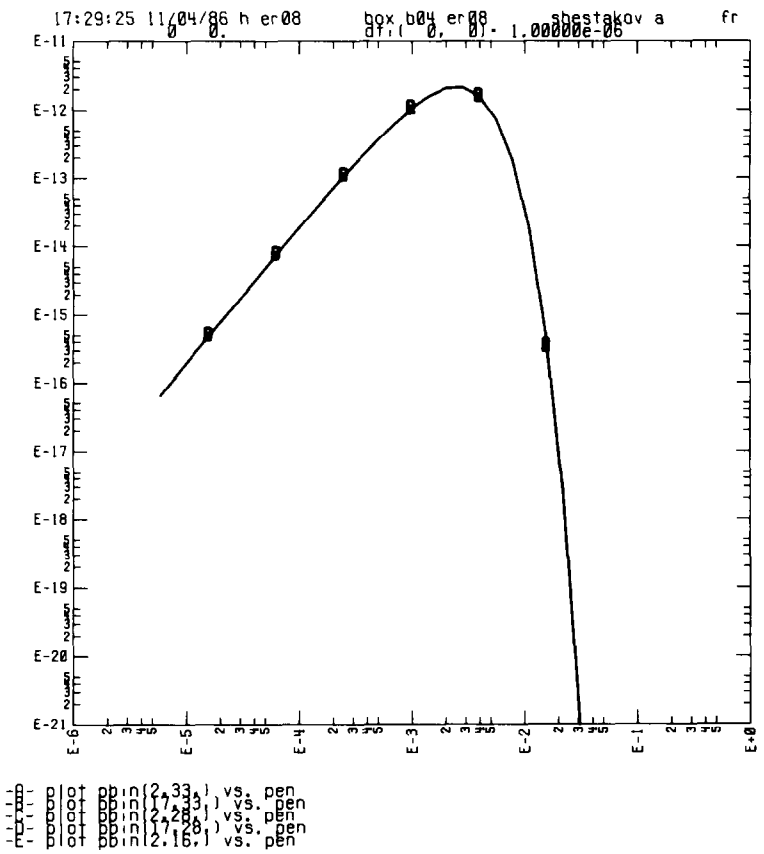

FIG. 10. Problem 4. Photon energy density distribution (ergs $\times 10^{16}$/cm^3/keV) is the abscissa, photon energy (keV) is the ordinate.

During the run, the radiation field loses more than 38% of its energy while T_e remains relatively unchanged. Hence, the opacities of Fig. 9 remain constant for the duration of the run. The total energy fluence leaving the problem, however, is over half that of the original radiation energy. Approximately 30% of the fluence comes from the electrons which have a considerably larger reservoir of energy.

Results are displayed in Table II. Run names beginning with "d" or "e" respectively categorize the FD or FE schemes. The second character, "o" or "r" denotes an orthogonal or a random mesh. The last two numbers, "33" or "65," define the mesh size, 33×33 or 65×65. The runs on the large mesh are used to benchmark the solution; note the good agreement between "do65" and "eo65."

It is interesting to examine Table II. On a random mesh, FD has tremendous variations between zones, yet the domain averaged answers are surprisingly good. The fluxes, in particular, vary nearly an order of magnitude along the outer edge

TABLE II

Comparison of Runs on Problem 4 at $t = 0.020932643$

Run	E_r	Flxc ($r = 10$)	Fluc ($r = 10$)	T_r ($r = 10$)	Flx ($r = 10$)
do33	8.203 + 4	2 7891 + 6	7 2415 + 4	0.75610	6.278 + 3
dr33	7 904	2 9075	7 6737	0 7483 to 0 7407	17.84 to 2.109
do65	8 156	2 8109	7.3175	0 75182	6.326
eo33	8.107	2.8472	7.4243	0.75242	6.408
er33	8 103	2 8456	7 4216	0.7557 to 0.7493	6.419 to 6.392
eo65	8.109	2.8421	7 4126	0.74989	6.397

Note. Variables and units: E_r(ergs), radiation energy in domain; Flxc (ergs/τ), net escaped flux; Fluc (ergs), net escaped fluence; T_r (eV), radiation temperature per zone or point along $r = 10$; Flx (ergs/cm^2/τ), flux per zone or point along $r = 10$. Notation in first row: $8.203 + 4$ signifies 8.203×10^4. Orders of magnitude are the same for the column entries, i.e., E_r for eo65 is 8.109×10^4 ergs.

($r = 10$), yet the total flux and fluence are respectively only 4% and 6% greater than "do33." The FE method is considerably better behaved. The relative differences, Eq. (35), in the fluxes are respectively 1.57 and 0.004 for the FD and FE methods, a dramatic improvement. In addition, FE is apparently more accurate on the orthogonal mesh for its results on "o33" and "o65" are nearly identical. For this transport-dominated problem the increased accuracy of FE is self-evident.

5. Conclusion

We have presented a diffusion scheme using the finite element method which may be integrated into a Lagrangian hydrodynamic code. Results on test problems on fixed but irregular meshes illustrate the increased accuracy of FE. In contrast to the usual zone-averaged methods the method calculates nodal quantities. Care must be exercised in coupling to other zonal variables. In particular, straightforward coupling to a zonal electron temperature can result in anomalously large diffusion. It is fair to end with a word of caution. The FE method is based on triangles and does not rely on mapping to a logical (K, L) space. Hence, it will not maintain the exact symmetry that the FD scheme preserves when it is used on orthogonal meshes. In particular, an alternating bisection strategy for the quadrilaterals is implemented at initialization in regions where the grid lines are straight. This prevents the calculation from developing a "bias."

We end with a few words about comparative timings. We have not noticed a significant difference in the running times between the FE and FD schemes. The two are usually within 20% of each other. For some problems, FE is faster; for others slower. We recall that the nodal FE is being compared to a zonal one. A problem of $KMAX \times LMAX$ grid points has to update that many nodal values, but encloses only $KMAX \times LMAX - (KMAX + LMAX - 1)$ zones. When $KMAX$ and

LMAX are both large the difference is insignificant. The difference increases as one problem dimension is much larger than the other. For the extreme case, e.g., $KMAX = 2$, there are over twice as many points as zones. However, in that case, the problem is one-dimensional and an appropriate one-dimensional FE scheme should be used.

ACKNOWLEDGMENTS

The FE package grew from extensive modifications and additions to a scalar parabolic equation solver written by Dr. Manoj K. Prasad of the Lawrence Livermore National Laboratory. In addition, conversations with Dr. Prasad were useful in clarifying certain obscure portions of the text. His contribution is gratefully acknowledged. Opacity tables for problem 4 were compiled from Ref. [10] by Dr. Minao Kamegai of the Lawrence Livermore National Laboratory. This document was prepared by Ms. Bonnie Quick of the Lawrence Livermore National Laboratory on a SUN workstation using the text editor EMACS and the formatters EQN, TBL, and MS of PTROFF. The paper profited greatly from careful readings and suggestions of the reviewers, most notably that of Dr. Barry D. Ganapol. Work performed under the auspices of the U.S. Department of Energy by the Lawrence Livermore National Laboratory under Contract W-7405-ENG-48.

REFERENCES

1. D. S KERSHAW, *J. Comput. Phys.* **39**, No. 2, 375 (1981).
2. G C POMRANING, *Radiation Hydrodynamics* (Pergamon, Oxford, 1973).
3. G. STRANG AND G. FIX, *Analysis of the Finite Element Method* (Prentice-Hall, Englewood Cliffs, NJ, 1973).
4. R. S VARGA, *Matrix Iterative Analysis* (Prentice-Hall, Englewood Cliffs, NJ, 1962).
5. C. D. LEVERMORE AND G C. POMRANING, *Astrophys. J.* **248**, No. 1, 321 (1981).
6. C D. LEVERMORE, *J. Quant. Spectrosc. Radiat. Transfer* **31**, No. 2, 149 (1984).
7. G. J. PERT, *J. Comput. Phys.* **42**, 20 (1981).
8. Y. B. ZEL'DOVICH AND Y. P. RAIZER, *Physics of Shock Waves and High-Temperature Hydrodynamic Phenomena II* (Academic Press, New York, 1967), p. 668.
9. Y B. ZEL'DOVICH AND Y. P. RAIZER, *Physics of Shock Waves and High-Temperature Hydrodynamic Phenomena II* (Academic Press, New York, 1967), p. 611.
10 R R. JOHNSTON AND D E. STEVENSON, Sci. Appl. Inst. Rep. SAI-056-77-PA, June 1977 (unpublished).